JOURNAL OF SOLID STATE CHEMISTRY **136,** 67–73 (1998)
ARTICLE NO. SC977657

Phase Transitions of Ti_3O_5

Masashige Onoda

Institute of Physics, University of Tsukuba, Tennodai, Tsukuba 305, Japan

Received March 21, 1997; in revised form June 26, 1997; accepted October 12, 1997

The crystal structure and electronic state of Ti_3O_5, which undergoes first-order structural and magnetic–nonmagnetic transitions at 460 K on heating and 440 K on cooling, have been explored through X-ray four-circle diffraction, magnetic, and transport measurements. A successive monoclinic ($C2/m$)–orthorhombic transition appears at about 500 K. The crystal structure at 514 K has been determined with $R = 0.040$ and $R_w = 0.038$ for 1027 independent reflections, where the space group is *Cmcm* with lattice constants $a = 3.798(2)$ Å, $b = 9.846(3)$ Å, and $c = 9.988(4)$ Å, and $Z = 4$. The structure is basically built up of a linkage of distorted TiO_6 octahedra and is of a pseudobrookite type. Each effective Ti valence is nearly equal to an average value. These characteristics are nearly consistent with magnetic and transport properties. Ti_3O_5 in the orthorhombic phase is like a highly correlated metal.

I. INTRODUCTION

Various properties of transition metal oxides arise from their crystal structures, which are generally formed by the linkage of rigid units such as TO_6 octahedra or TO_4 tetrahedra, where T is the transition metal ion. Electrons located in TO_n cage bands contribute to transport, the properties of which strongly depend on the species of the T ions. In particular, $3d$ transition metal oxides or bronzes are considered to be located near the metal–insulator phase boundary with a significant electron–electron correlation and/or an electron–phonon coupling (1–4).

Titanium binary oxides with unfilled $3d$ orbitals, such as Ti_3O_5 ($TiO_{1.66}$) and the homologous series Ti_nO_{2n-1} ($TiO_{2-1/n}$; $n \geq 4$), are known to undergo phase transitions of crystal structures, electron transport, or magnetic properties (5–18). Among these compounds, Ti_4O_7 has been studied intensively to clarify interesting aspects of strong electron–phonon coupling systems.

The crystal structure of Ti_3O_5 at room temperature, hereafter called the LM structure, was determined by Åsbrink and Magnéli (5). It is monoclinic with space group $C2/m$ and the lattice constants are $a = 9.752(1)$ Å, $b = 3.802(1)$ Å, $c = 9.442(1)$ Å, and $\beta = 91.55(1)^\circ$. The structure is shown in Fig. 1 using the numbering scheme of ref 5. The Ti atoms have three crystallographically independent sites, labeled Ti1, Ti2, and Ti3, that are octahedrally surrounded by oxygen atoms. The structure is viewed in terms of distorted TiO_6 octahedra that are linked by sharing edges and corners to form an infinite three-dimensional framework. In the *ac* plane, there is a characteristic row of six edge-sharing octahedra running along the $\langle \bar{1}03 \rangle$ direction. This is linked to the adjacent two rows by sharing three edges in the *ac* plane and its extension along the *b* axis is realized by octahedra sharing corners. The Ti–Ti pairs with distance smaller than a critical distance $r_c \simeq 2.90$ Å, which is a mean value in α- and β-Ti metals, are located in the *ac* plane. Effective mean Ti valences are 3.0, 3.7, and 3.3 for the atoms in the Ti1, Ti2, and Ti3 sites, respectively.[1] Therefore, $3d^1$ electrons are approximately located at the Ti1 and Ti3 sites but absent at the Ti2 site.

Phase transitions of Ti_3O_5 have been investigated through measurements of lattice constants, electrical resistivity, and magnetic susceptibility (5–13). Although some disagreements among the results exist, the general features of the phase transition may be summarized as follows: The transition is of the first order accompanied with a rapid decrease of resistivity and a rapid increase of the *c* axis and the magnetic susceptibility on heating. The transition temperature T_c is approximately 460 K on heating. Available resistivity results indicate that Ti_3O_5 has a semiconductor-like conduction below T_c, but it appears difficult to conclude whether the phase above T_c is metallic.

According to the LM structure shown in Fig. 1 and an empirical theory of Goodenough (19), Mulay and Danley (11) considered a model of constrained-type antiferromagnetism that sets in between specific neighboring *d* electrons through homopolar bonding between Ti^{3+} ions as a cause of the nonmagnetic state below T_c. This model postulates that the electrons are delocalized within the Ti^{3+}–Ti^{3+} bonds. However, it may also be viewed as antiferromagnetically exchange-coupled pairs, between which the exchange coupling is not significant.

[1] These values are obtained in the same way as described in section II by using atomic parameters refined by the present study. An analysis based on parameters determined by Åsbrink and Magnéli (5) also provides similar results.

0022-4596/98 $25.00

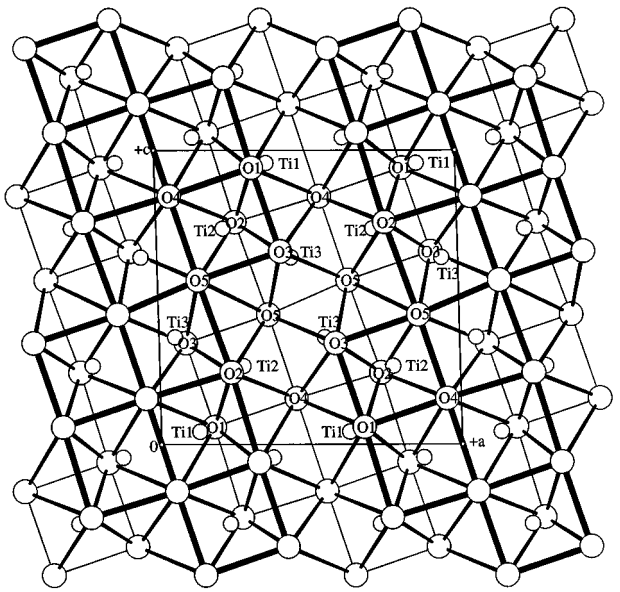

FIG. 1. Crystal structure of Ti_3O_5 at 296 K projected on the monoclinic *ac* plane. The thick and thin lines correspond to the edges in the planes at $y = 0$ and $\frac{1}{2}$, respectively, of the oxygen octahedra.

No direct structure determination of Ti_3O_5 above T_c has been carried out. However, Åsbrink and Magnéli (5) postulated based on X-ray powder diffraction patterns that the phase above T_c is of the anosovite type determined by Ždanov and Rusakov on a sample containing considerable amounts of elements other than Ti and O (6) and a slightly deformed pseudobrookite structure. The lattice constants above T_c are monoclinic with $a = 9.82$ Å, $b = 3.78$ Å, $c = 9.97$ Å, and $\beta = 91.0°$, whereas those of the anosovite are orthorhombic with $a = 3.754(1)$ Å, $b = 9.474(1)$ Å, and $c = 9.734(2)$ Å. Therefore, the unit cell of Ti_3O_5 above T_c is approximately related to that of the anosovite as follows:

$$\begin{pmatrix} a \\ b \\ c \end{pmatrix}_{T > T_c} = \begin{pmatrix} 0 & 1 & 0 \\ -1 & 0 & 0 \\ 0 & 0 & 1 \end{pmatrix} \begin{pmatrix} a \\ b \\ c \end{pmatrix}_{\text{anosovite}} . \qquad [1]$$

This means that the phase transition of Ti_3O_5 is suppressed by a slight substitution of Ti with Fe, which has been reported in ref 5.

To clarify the detailed mechanism of the transition and the electronic properties, it is necessary to determine the crystal structure of *pure* Ti_3O_5 above T_c. Section II describes the crystal structure above T_c and the temperature dependence of the lattice constants. In section III, magnetic and transport properties are discussed based on the crystal structures. A conclusion for the phase transitions and electronic state of Ti_3O_5 is given in section IV.

II. CRYSTAL STRUCTURES

A. Experiments

Polycrystalline specimens of Ti_3O_5 were first prepared from a mixture of a 1 : 2 molar ratio of Ti metal (99.9% purity) and TiO_2 (99.9% purity) in an electric arc furnace under an Ar atmosphere. Single crystals were prepared by heating the polycrystalline specimens in a sealed evacuated quartz tube at 1373 K for 10 days and then by cooling them slowly in the furnace.

X-ray powder diffraction patterns for the polycrystalline specimens were taken on a Rigaku RAD-IIC diffractometer with Cu$K\alpha$ radiation at room temperature. X-ray four-circle diffraction measurements were carried out on a Rigaku AFC-7R diffractometer (custom made) with graphite-monochromated Mo$K\alpha$ radiation and an 18-kW rotating-anode generator in the temperature region between 290 and 550 K. Temperatures at the sample were controlled by an N_2 gas flow system within an accuracy of 0.5 K. A crystal with dimensions $0.10 \times 0.02 \times 0.17$ mm was mounted on a glass fiber.

The lattice constants and the orientation matrix were obtained from a least-squares refinement using setting angles of 25 carefully centered reflections in the 2θ range near 50°. Intensity data for the structure analysis were collected at 514 K using the ω–2θ scan technique and those at 296 K were measured to improve the accuracy of the atomic parameters. Data at intermediate temperatures were also collected roughly to check the systematic absences of reflections and intensity distribution.

B. Results

1. Lattice constants. X-ray powder diffraction patterns for the polycrystalline specimens at room temperature corresponded to those reported by Andersson *et al.* (7). Based on the systematic absences of reflections for single-crystal diffraction, a statistical analysis of intensity distribution, and the successful solution and refinement of the structure described later, the space groups and the lattice constants at 514 and 296 K are determined as listed in Table 1. The results at 296 K are consistent with previous results (5). On the other hand, the data at 514 K are orthorhombic, which differs from the results that indicate a monoclinic cell.

The lattice constants as a function of temperature are shown in Fig. 2a. The temperature dependence of the lattice constant ratio, defined as $\Delta = p/p_0 - 1$, where p is the lattice constant at a given temperature and p_0 is that at 296 K, respectively, is shown in Fig. 2b. Here, we follow the assignment of crystal axes at 296 K for convenience, where a, b, and β at 296 K correspond to b, a, and α at 514 K, respectively, according to Eq. [1].

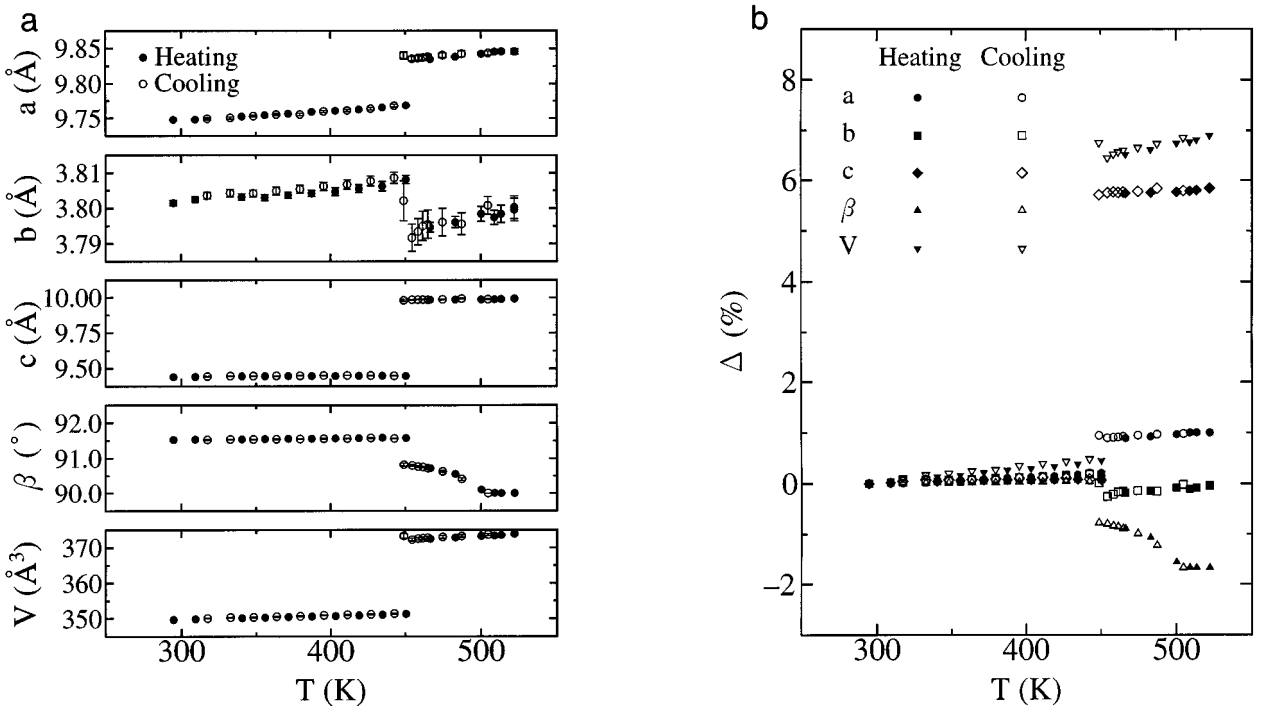

FIG. 2. (a) Temperature dependence of the lattice constants of Ti_3O_5. (b) Temperature dependence of the relative changes Δ of the lattice constants from the values at 296 K.

2. Structure refinements and determination. An empirical absorption correction based on azimuthal scans of several reflections and corrections for Lorentz–polarization and secondary extinction effects were applied to the reflection data. Various parameters for structure solutions and refinements are summarized in Table 2.

The structures were solved by direct methods (20), expanded using Fourier techniques, and refined by full-matrix least-squares calculations with anisotropic displacement parameters. Here, atomic scattering factors were taken from Cromer and Waber (21), and anomalous dispersion effects were included, for which the values were those of Creagh and McAuley (22). All calculations were performed using the teXsan crystallographic software package (23).

There is no significant difference between the atomic coordinates for the LM structure refined by the present and previous works (5), but the accuracy of atomic parameters is

TABLE 1
Crystal Data of Ti_3O_5 at 514 and 296 K

	514 K	296 K
Crystal system	Orthorhombic	Monoclinic
Space group	*Cmcm* (No. 63)	*C*2/*m* (No. 12)
Z value	4	4
a (Å)	3.798(2)	9.748(1)
b (Å)	9.846(3)	3.8013(4)
c (Å)	9.988(4)	9.4405(7)
β		91.529(7)
V (Å^3)	373.5(2)	349.69(6)
$\mu_{MoK\alpha}$ (mm^{-1})	6.152	6.572
D_{cal} (Mg/m^3)	3.977	4.249

TABLE 2
Summary of Intensity Measurements, Structure Solutions, and Refinements of Ti_3O_5 at 514 and 296 K

	514 K	296 K
Radiation	Mo*K*α	Mo*K*α
$2\theta_{max}$ (deg)	120	120
No. of unique reflections	1628	2865
R_{int}	0.019	0.019
Corrections	Lorentz–polarization Absorption (trans: 0.65–1.00) Secondary extinction[a] (coef: $2.2(1)\times10^{-6}$)	Lorentz–polarization Absorption (trans: 0.65–1.00) Secondary extinction (coef: $2.39(3)\times10^{-6}$)
Structure solution	Direct method (SAPI 91)	Direct method (SAPI 91)
Refinement	Full-matrix least-squares	Full-matrix least-squares
No. of observations ($I > 3\sigma$)	1027	2327
No. of variables	28	50
Reflection/parameter ratio	36.68	46.54
R^b	0.040	0.027
$R_w{}^c$	0.038	0.028

[a] $|F_c| = S|F_o|(1 + g|F_c|^2)$, where S and g are a scale factor and a coefficient for the secondary extinction correction, respectively.

[b] $R = \sum||F_o| - |F_c||/\sum|F_o|$

[c] $R_w = [\sum w(|F_o| - |F_c|)^2/\sum wF_o^2]^{1/2}$.

TABLE 3
Atomic Coordinates,[a] Equivalent Isotropic Thermal Parameters B_{eq} (Å^2),[b] and Anisotropic Displacement Parameters U_{ij}[c] of Ti_3O_5 at 514 K

Atom	Site	y	z	B_{eq}	U_{11}	U_{22}	U_{33}	U_{13}
Ti1	8*f*	0.63376(4)	0.55982(5)	0.755(5)	0.0078(1)	0.0088(1)	0.0121(1)	0.0007(1)
Ti2	4*c*	0.69515(6)	$\frac{1}{4}$	0.701(7)	0.0090(2)	0.0087(2)	0.0089(2)	
O1	8*f*	0.1851(2)	0.5687(2)	0.91(2)	0.0094(6)	0.0134(6)	0.0119(7)	−0.0013(5)
O2	8*f*	0.5484(2)	0.3798(2)	1.28(3)	0.0263(10)	0.0109(6)	0.0116(7)	0.0019(6)
O3	4*c*	0.7369(3)	$\frac{3}{4}$	0.93(3)	0.0097(8)	0.0157(10)	0.0098(8)	

[a] For all atoms, $x = 0$ and $U_{12} = U_{23} = 0$.
[b] $B_{eq} = \frac{8}{3}\pi^2[U_{11}(aa^*)^2 + U_{22}(bb^*)^2 + U_{33}(cc^*)^2 + 2U_{12}aa^*bb^*\cos\gamma + 2U_{13}aa^*cc^*\cos\beta + 2U_{23}bb^*cc^*\cos\alpha]$.
[c] $T = \exp[-2\pi^2(a^{*2}U_{11}h^2 + b^{*2}U_{22}k^2 + c^{*2}U_{33}l^2 + 2a^*b^*U_{12}hk + 2a^*c^*U_{13}hl + 2b^*c^*U_{23}kl)]$.

considerably improved. The structure shown in Fig. 1 is by the present work. Tables of observed and calculated structure factors of Ti_3O_5 at 514 and 296 K have been deposited with the National Auxiliary Publications Service (NAPS).[2]

The final results of atomic coordinates, equivalent isotropic thermal parameters, and anisotropic displacement parameters for the crystal structures at 514 K are listed in Table 3 and those at 296 K have been deposited with NAPS.[2] Figure 3 indicates the structure of pure Ti_3O_5 at 514 K. Selected interatomic distances are listed in Table 4.

C. Discussion

As shown in Figs. 2a and 2b, an abrupt change in the lattice constants appears at $T_c = 460$ K on heating and at 440 K on cooling, indicating a first-order transition. The thermal hysteresis width is approximately 20 K. Between T_c and 500 K, β is *not* equal to $\pi/2$ and depends on temperature, while other axis parameters are nearly temperature independent. In this temperature region, the space group is $C2/m$. Therefore, a successive monoclinic ($C2/m$)–orthorhombic (*Cmcm*) transition exists at about 500 K. The high-temperature monoclinic structure claimed by Åsbrink and Magnéli (5), hereafter called the HM structure, likely corresponds to the phase with $C2/m$ between T_c and 500 K.

The orthorhombic crystal structure at 514 K, hereafter called the HO structure, basically corresponds to that of anosovite or is of the pseudobrookite type as found from Fig. 3. There exist two crystallographically independent Ti sites, labeled Ti1 and Ti2, both of which are octahedrally surrounded by oxygen atoms. The TiO_6 octahedra form a characteristic row extending along the c axis, which is joined to an adjacent row by sharing corners and edges. The

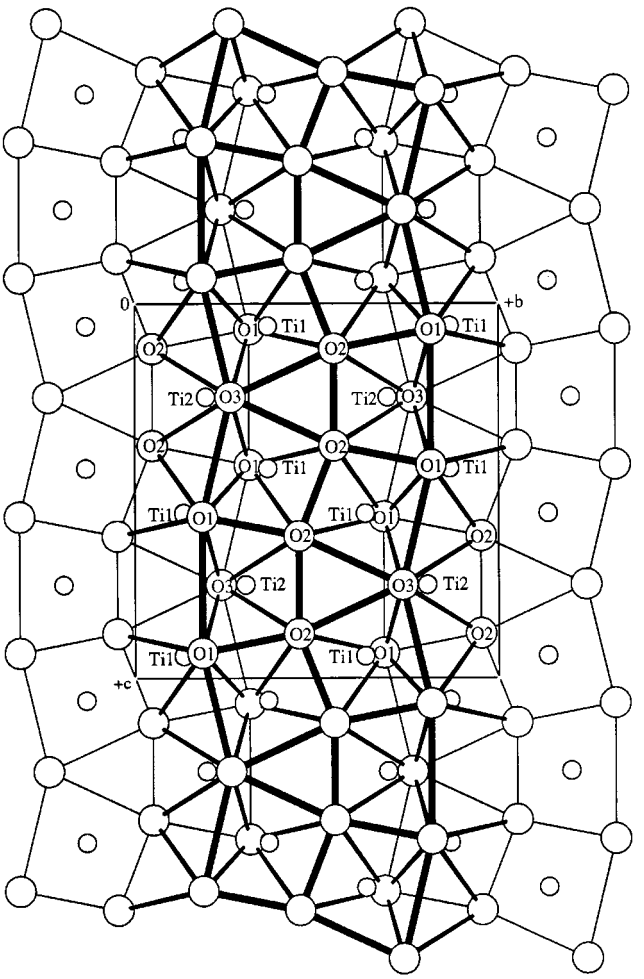

FIG. 3. Crystal structure of Ti_3O_5 at 514 K projected on the orthorhombic *bc* plane. The thick and thin lines correspond to the edges in the planes at $x = 0$ and $\frac{1}{2}$, respectively, of the oxygen octahedra.

[2] See NAPS document No. 05445 for 26 pages of supplementary material. This is not a multi-article document. Order from NAPS c/o Microfiche Publications, P.O. Box 3513, Grand Central Station, New York, NY 10163-3513. Remit in advance in U.S. funds only $9.55 for photocopies or $5.00 for microfiche. There is a $25.00 invoicing charge on all orders filled before payment. Outside U.S. and Canada add postage of $4.50 for the first 20 pages and $1.00 for each 10 pages of material thereafter, or $1.75 for the first microfiche and $1.00 for each microfiche thereafter.

TABLE 4
Selected Interatomic Distances (Å) of Ti_3O_5 at 514 K

Ti1[a]–Ti1[b,c]	3.205(1)	Ti2[a]–O3[b,c]	2.014(2)
–Ti1[d]	2.892(1)	O1[a]–O1[i,j]	2.669(3)
–Ti2[a]	3.1529(5)	–O2[k,l]	2.996(2)
–Ti2[b,c]	3.1706(9)	–O2[i,j]	3.025(2)
–O1[e,f]	1.967(1)	–O2[d]	2.675(3)
–O1[d]	2.198(2)	–O3[k,l]	2.673(2)
–O2[a]	1.985(2)	–O3[d]	3.275(2)
–O2[d]	1.892(2)	O2[a]–O2[h]	2.594(4)
–O3[a]	2.154(1)	–O2[d]	2.583(4)
Ti2[a]–O1[g,d]	2.161(2)	–O3[b,c]	3.124(3)
–O2[a,h]	1.942(2)	–O3[d]	3.094(3)

[a] x, y, z.
[b] $-\frac{1}{2}+x, \frac{3}{2}-y, 1-z$.
[c] $\frac{1}{2}+x, \frac{3}{2}-y, 1-z$.
[d] $x, 1-y, 1-z$.
[e] $\frac{1}{2}+x, \frac{1}{2}+y, z$.
[f] $-\frac{1}{2}+x, \frac{1}{2}+y, z$.
[g] $x, 1-y, -\frac{1}{2}+z$.
[h] $x, y, \frac{1}{2}-z$.
[i] $-\frac{1}{2}+x, \frac{1}{2}-y, 1-z$.
[j] $\frac{1}{2}+x, \frac{1}{2}-y, 1-z$.
[k] $-\frac{1}{2}+x, -\frac{1}{2}+y, z$.
[l] $\frac{1}{2}+x, -\frac{1}{2}+y, z$

extension of the a axis is formed by octahedra sharing corners. The TiO_6 octahedra share six edges with their neighbors. The displacement parameters of all the atoms may be normal as found in Table 3. The Ti–Ti distances in Table 4 are classified into two groups: 2.89 and 3.15–3.21 Å. The shortest pair exists between the Ti1 atoms in the bc plane and is comparable to r_c. The distances in the latter group are too large for significant direct overlap of the titanium 3d wavefunctions.

The valence distribution of Ti_3O_5 may be estimated basically with the critical overlap integral between the titanium and oxygen atoms. From the results of Table 4, the bond strengths and the effective mean valences for the Ti1 and Ti2 octahedra are determined as listed in Table 5 in terms of the bond length versus bond strength relation (24). The difference between the Ti1 and Ti2 valences is small and the average valence is consistent with $Ti^{3.33+}$ expected from the chemical formula. This indicates that Ti_3O_5 in the orthorhombic phase is like a metal and undergoes a valence order of Ti ions in the LM structure. The O valence is close to the closed-shell value.

TABLE 5
Bond Strength and Effective Mean Ti and O Valences of Ti_3O_5 at 514 K

	Ti1	Ti2	v(O)
O1	0.641[a,b] 0.314	0.352[a]	1.95
O2	0.607 0.808	0.693[a]	2.11
O3	0.360[b]	0.555[a,b]	1.83
v(Ti)	3.37	3.20	

[a] Two symmetry-related O atoms are bonded to the Ti atom.
[b] Two symmetry-related Ti atoms are bonded to the O atom.

As previously suggested (5), a rotation of the Ti–Ti pair with the distance 2.89 Å in the bc plane and a displacement of the neighboring O atoms are essential for the structural transition at T_c based on the comparison between Figs. 1 and 3. Between T_c and 500 K, this displacement is small but still active.

III. MAGNETIC AND TRANSPORT PROPERTIES

A. Experiments and Results

The electrical resistivity ρ of the single crystals was measured by a dc four-terminal method in the temperature region between 80 and 650 K. The specimen was first cooled to 80 K, then heated to 650 K, and finally cooled to about 160 K. Here, measurements in the region above 300 K were done in a vacuum and those below 300 K were made in a glass dewar using liquid N_2. The temperature dependence of ρ on heating and cooling is shown in Fig. 4. The resistivity data for the first cooling process below 300 K agree with

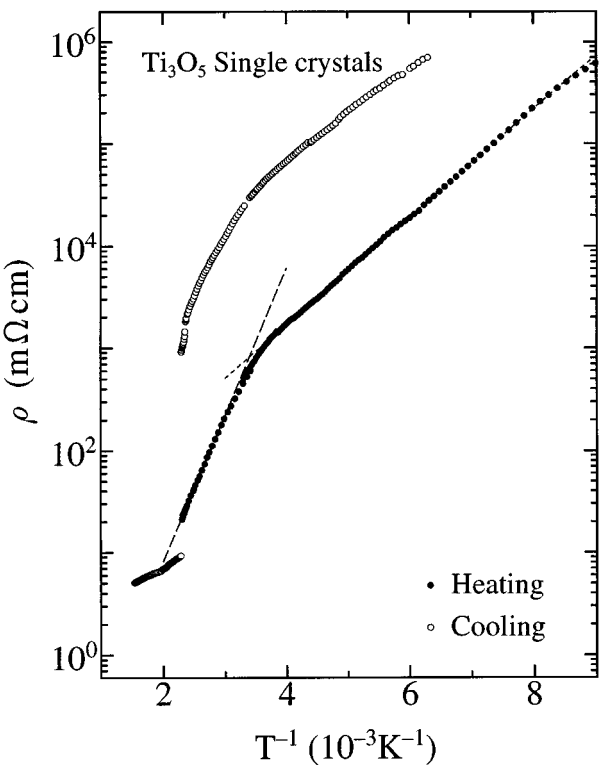

FIG. 4. Temperature dependence of the electrical resistivity ρ of Ti_3O_5.

those for the first heating process. Since the data above T_c for the first heating process are scattered a little owing to the large change in the unit cell parameters as described earlier, they are not plotted. The data for the cooling process from 650 K may be more reliable, because the crystals were annealed at 650 K, well above T_c, to remove cracks in the crystal as much as possible.

Magnetization in the region below 10 kOe for the polycrystalline specimens was measured by the Faraday method between 4.2 and 850 K. The specimen was cooled to 4.2 K, and then heated to 900 K, and finally cooled to 300 K, where measurements above 300 K were made done in a vacuum and those below 300 K were made in a glass dewar using liquid He. Temperatures at the sample were stabilized within 1 K.

The magnetization field curve was linear and thus the magnetic susceptibility χ was deduced from the slope of that curve. The temperature dependence of χ on heating and cooling is shown in Fig. 5. The susceptibility data for the first cooling process below 300 K agree well with those for the first heating process. No significant change in X-ray powder diffraction patterns at room temperature was observed after the magnetic measurements.

B. Discussion

As shown in Fig. 4, a significant jump as well as a thermal hysteresis of the resistivity exists, which is consistent with a first-order phase transition. T_c's in this measurement agree with the values described earlier. The magnitude of the resistivity below T_c on heating is different from that on cooling through T_c. This may likely be attributed to a difference of the effective cross-sectional area of the specimens due to the large changes of the unit cell parameters at the transition, since we know that cracking often happens when a specimen is heated through T_c. Therefore, it is difficult to estimate the precise magnitude of the resistivity. In other words, the intrinsic magnitude of the resistivity should be smaller than that described here. The temperature dependence below T_c is semiconductor-like and changes in the vicinity of 300 K. From the dashed and dotted lines of Fig. 4, the energy gap E_g/k, defined as $\rho = \rho_0 \exp(E_g/kT)$, where ρ_0 is assumed to be a constant and k is the Boltzmann constant, is estimated to be 3300 K between T_c and 330 K and 1200 K below 250 K. This tendency appears to exist in the cooling process through T_c as well. It is reminiscent of variable-range hopping-like conduction (25), in which the density of states at the Fermi level is finite. However, internal flaws due to a structural transition will give rise to similar behaviors. This problem should be clarified by another experiment such as high-frequency conductivity measurements. On the other hand, in the region above T_c, the temperature dependence of the resistivity still appears to be nonmetallic, but it is not clear whether this is inherent. At about 500 K, the monoclinic (HM)–orthorhombic (HO) transition temperature, a small anomaly of the resistivity exists.

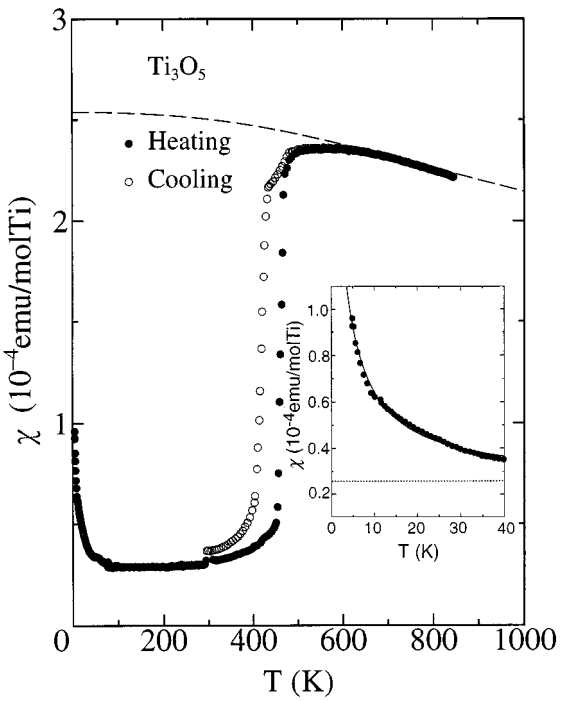

FIG. 5. Temperature dependence of the magnetic susceptibility χ of Ti_3O_5. The inset shows the low-temperature behavior.

Figure 5 shows a large jump and a thermal hysteresis of the susceptibility. T_c's on heating and cooling are 460 and 430 K, respectively. The hysteresis width is slightly larger than those estimated from measurements of the lattice constants and the resistivity, which is likely due to a difference of measurement times at each temperature.

The susceptibility between T_c and about 100 K is nearly temperature independent, 3×10^{-5} emu/mol of Ti, but at lower temperatures, it has a Curie–Weiss-like tail due to magnetic impurities or lattice imperfections as indicated in the inset of Fig. 5. From the solid line of the inset, the Curie constant and Weiss temperature are estimated to be 4.5×10^{-4} emu K/mol of Ti and 1 K, respectively. The constant paramagnetism χ_0, which consists of the Van Vleck paramagnetism and the diamagnetism, is $\chi_0 = 2.6 \times 10^{-5}$ emu/mol of Ti as indicated by the dotted line. The decrease of magnetic susceptibility means a formation of spin-singlet pairs or clusters of electrons as proposed previously (11). A relative gain of magnetic energy may stabilize the LM structure. In such a sense, this transition is similar to characteristic phenomena in low-dimensional compounds such as the *bipolaron* in β-$Na_xV_2O_5$ with $x \simeq \frac{1}{3}$ or the *trimer* in $LiVO_2$ (26, 27).

The susceptibility above T_c takes a maximum in the vicinity of 550 K, much higher than T_c. Since in this

temperature region, χ_0 as well as the d spin susceptibility χ_d contributes to the susceptibility, this result suggests the existence of a pseudogap for the density of states in the metallic region. Using a free-electron relationship for simplicity, χ_d corresponds to a Pauli paramagnetic susceptibility $\chi_P = N\mu_B^2(kT)^{-1}F'_{1/2}(\xi)/F_{1/2}(\xi)$, where N and μ_B are the number of electrons and Bohr magneton, respectively, and $F_{1/2}(\xi) = \int x^{1/2}/[\exp(x-\xi)+1]dx$ with $\xi = E_F/kT$, E_F being the Fermi energy (28). The dashed line in Fig. 5 is based on the parameters $E_F/k = 2040$ K and $\chi_0 = 7 \times 10^{-5}$ emu/mol of Ti. This model accounts for the results above 600 K qualitatively. A significant reduction of E_F corresponds to an enhancement of effective carrier mass, $m_{eff} = 16m_0$, m_0 being a free-electron mass. Here, a contribution from the Landau diamagnetism is negligible and we have assumed that the Wilson ratio is nearly unity. A difference between the Van Vleck susceptibilities in the magnetic and nonmagnetic states may be attributed to the structural transition or the valence order of Ti ions.

In the cooling process, a characteristic decrease of the susceptibility with decreasing temperature exists between T_c and about 500 K. It is not clear in the heating process, but a distinct change in the susceptibility is found at about 500 K. This may be correlated with the temperature dependence of the monoclinic angle β or the HM–HO transition as revealed before.

IV. CONCLUSION

The structural and electronic properties of Ti_3O_5 have been studied through X-ray four-circle diffraction, magnetic, and transport measurements. A first–order structural transition at $T_c = 460$ K on heating and at 440 K on cooling corresponds to the LM ($C2/m$)–HM($C2/m$) transition. A successive HM–HO ($Cmcm$) transition appears at about 500 K. The crystal structure at 514 K or the HO structure is basically built up of a linkage of distorted TiO_6 octahedra and is of the pseudobrookite type. Each effective Ti valence is nearly equal to an average value.

The structural characteristics are consistent with magnetic and transport properties. A large jump of the susceptibility and resistivity appears at the LM–HM transition and a small anomaly takes place at the HM–HO transition. Both transitions lead to a magnetic energy gain in the state below each transition temperature. The electronic state with the HO structure has a pseudogap for the density of states and a significant electron correlation. Thus, Ti_3O_5 in the orthorhombic phase is like a highly correlated metal. Unfortunately, due to the large structural transition, the present resistivity measurements do not provide specific results of the conduction mechanism.

The existence of the structural transition suggests that an electron–phonon coupling effect also plays an important role in the metal–semiconductor and magnetic–nonmagnetic transitions. Generally, this effect does not compete with the correlation effect and therefore it is not easy to reach a definite conclusion regarding the electronic state of Ti_3O_5.

ACKNOWLEDGMENT

Mr. Y. Ogawa is gratefully acknowledged for his help in the magnetic measurements.

REFERENCES

1. J. B. Goodenough, *Prog. Solid State Chem.* **5,** 149 (1971).
2. N. Tsuda, K. Nasu, A. Yanase, and K. Siratori, "Electronic Conduction in Oxides." Springer-Verlag, Berlin, 1991.
3. N. F. Mott, "Metal–Insulator Transitions," 2nd ed. Taylor & Francis, London, 1990.
4. A. Georges, G. Kotliar, W. Krauth, and M. Rozenberg, *Rev. Mod. Phys.* **68,** 13 (1996).
5. S. Åsbrink and A. Magnéli, *Acta Crystallogr.* **12,** 575 (1959).
6. G. S. Ždanov and A. A. Rusakov, *Struct. Rep.* **18,** 459 (1954); *Trudy Inst. Krist. Akad. Nauk SSSR* **9,** 165 (1954).
7. S. Andersson, B. Collén, G. Kruuse, U. Kuylenstierna, A. Magnéli, H. Pestmalis, and S. Åsbrink, *Acta Chem. Scand.* **11,** 1653 (1957).
8. G. Åsbrink and A. Magnéli, *Acta Chem. Scand.* **21,** 1977 (1967).
9. K. F. Bartholomew and D. R. Frankl, *Phys. Rev.* **187,** 828 (1969).
10. H. Iwasaki, N. F. H. Bright, and J. F. Rowland, *J. Less-Common Met.* **17,** 99 (1969).
11. L. N. Mulay and W. J. Danley, *J. Appl. Phys.* **41,** 877 (1970).
12. C. N. R. Rao, S. Ramdas, R. E. Loehman, and J. M. Honig, *J. Solid State Chem.* **3,** 83 (1971).
13. S. Åsbrink and A. Pietraszko, *Phys. Status Solidi A* **128,** K77 (1991).
14. S. H. Song and S. Åsbrink, *Acta Crystallogr. B* **38,** 2570 (1982).
15. I. E. Grey, C. Li, and I. C. Madsen, *J. Solid State Chem.* **113,** 62 (1994).
16. A. D. Inglis, Y. Le Page, P. Strobe, and C. M. Hurd, *J. Phys. C* **16,** 317 (1983).
17. C. Schlenker and M. Marezio, *Philos. Mag. B* **42,** 453 (1980).
18. Y. Le Page and M. Marezio, *J. Solid State Chem.* **53,** 13 (1984).
19. J. B. Goodenough, *Czech. J. Phys. B* **17,** 304 (1967).
20. F. Hai-Fu, "SAPI91: Structure Analysis Programs with Intelligent Control," Rigaku Corp., Tokyo, 1991.
21. D. T. Cromer and J. T. Waber, *in* "International Tables for X-Ray Crystallography" (J. A. Ibers and W. C. Hamilton, Eds.), Vol. IV, Sec. 2. Kynoch Press, Birmingham, 1974.
22. D. C. Creagh and W. J. McAuley, *in* "International Tables for Crystallography" (A. J. C. Wilson, Ed.), Vol. C. Kluwer Academic, Boston, 1992.
23. "Crystal Structure Analysis Package," Molecular Structure Corp., 1992.
24. W. H. Zachariasen, *J. Less-Common Met.* **62,** 1 (1978).
25. W. Brenig, G. H. Döhler, and P. Wölfle, *Z. Phys.* **258,** 381 (1973).
26. M. Onoda and H. Nagasawa, *Phys. Status Solidi B* **141** 507 (1987) and references therein.
27. M. Onoda and T. Inabe, *J. Phys. Soc. Jpn.* **62,** 2216 (1993) and references therein.
28. A. H. Wilson, "The Theory of Metals," 2nd ed. Cambridge Univ. Press, London, 1958.